Photoswitchable Antigen−Antibody Interactions Studied by Impedance Spectroscopy

Fernando Patolsky, Boris Filanovsky, Eugenii Katz, and Itamar Willner*

Institute of Chemistry and The Farkas Center for Light-Induced Processes, The Hebrew University of Jerusalem, Jerusalem 91904, Israel

Received: September 14, 1998

A thiolated dinitrospiropyran (**1a**) is assembled as a monolayer onto a Au electrode. The monolayer exhibits reversible photoisomerizable properties, and irradiation of the **1a** monolayer state, 360 nm < λ < 380 nm, yields the protonated merocyanine (**1b**) monolayer state, whereas illumination of the latter monolayer electrode, λ > 495 nm, regenerates the **1a** monolayer electrode. The **1a** monolayer interface acts as antigen for the dinitrophenyl antibody, DNP-Ab, while the **1b** state lacks an affinity for DNP-Ab. This stimulates the association of the antibody to the **1a** monolayer interface, while photoisomerization of the monolayer to the **1b** state allows one to wash off DNP-Ab and regenerate the **1a** monolayer assembly by a secondary illumination process. The photoisomerization of the monolayer interface and the binding or dissociation of DNP-Ab to and from the photoisomerizable monolayer are studied by impedance spectroscopy, in the presence or absence of a solubilized redox probe. The derived equivalent circuits enable us to characterize the monolayer parameters associated with the photoisomerization and the interactions of DNP-Ab with the monolayer. The non-Faradaic impedance measurements reveal only capacitance changes of the double-layer interface as a result of photoisomerization and the association of DNP-Ab to the monolayer. Faradaic impedance measurements using $[Fe(CN)_6]^{3-/4-}$ as a molecular redox probe or ferrocene-tethered glucose oxidase, GOx−Fc, and glucose as a bioelectrocatalytic redox probe, allow for the determination of the electron-transfer resistance, the electron-transfer rate constants, and the characteristic time constants of the equivalent circuits corresponding to the different states of the photoisomerizable monolayer in the absence and presence of DNP-Ab. Faradaic impedance appears to be an effective transduction signal for the photoisomerization occurring upon optical activation of the monolayer and for the photostimulated binding and dissociation of DNP-Ab to and from the monolayer, respectively. The system represents an optoelectronic "OR" gate.

Introduction

Construction of biological assemblies on electrode surfaces providing transduction of biological events into electronic signals is of substantial basic and practical importance for tailoring of biosensor,[1,2] immunosensor[3] and bioelectronic[4] devices. Integration of photoswitchable biomaterials with electronic transducers provides a means for the assembly of future optobioelectronic systems.[5,6] Several methods to organize optobioelectronic devices have been reported, including the chemical modification of redox proteins with photoisomerizable components and their immobilization on electrode supports[7,8] and the application of photoisomerizable monolayers associated with electrodes as command interfaces for photochemical control of the electrical contact of the proteins with the electrodes.[9,10] For example, chemical modification of glucose oxidase with nitrospiropyran photoisomerizable units[7] or reconstitution of apoglucose oxidase with a nitrospiropyran−FAD cofactor[8] led to photoswitchable redox enzymes that were assembled as monolayers onto electrode surfaces. A nitrospiropyran photoisomerizable monolayer associated with Au electrodes acted as a command surface for the light-stimulated control of the electrical contact of cytochrome c[9] or glucose oxidase[10] with the electrode support. In all of these systems, amperometric transduction of recorded optical signals was accomplished.

Photoisomerizable antigens were suggested as a means to tailor reversible and reusable immunosensor electrodes,[11,12] Scheme 1. By this approach, the antigen in photoisomer state **A** enables the sensing of the antibody by the electronic transduction of the formation of the antigen−antibody complex at the transducer surface. Upon completion of the sensing process, the active sensing layer is photoisomerized to state **B**. The latter configuration lacks antigen features for the antibody binding and allows one to wash off the associated antibody. By further photoisomerization of the state **B** to the original photoisomer state **A**, the antigen layer is regenerated for a secondary sensing cycle. According to this method, a reversible immunosensor electrode for the dinitrophenyl antibody, DNP-Ab, was assembled.[11,12] A dinitrospiropyran photoisomerizable monolayer assembled onto a Au electrode acted as the active antigen interface for sensing DNP-Ab. Photoisomerization of the monolayer to the protonated merocyanine state generated an interface lacking antigen properties for the DNP-Ab. This allowed one to wash off DNP-Ab, and by a subsequent photoisomerization of the monolayer to the dinitrospiropyran state, the active antigen assembly was recycled. Formation of the antigen−antibody complex at the sensing layer was electronically transduced using amperometric[11,12] or piezoelectric, quartz-crystal-microbalance signals.[12]

Impedance spectroscopy[13] is an effective method to probe the features of surface-modified electrodes and theoretical analyses[14] of the impedance properties of electrodes enable one to understand chemical transformations and processes associated with the conductive supports.[15] The hydrophobic nature of proteins suggests that formation of antigen−antibody complexes

* To whom correspondence should be addressed.

10.1021/jp983700n CCC: $15.00
Published on Web 11/13/1998

SCHEME 1: Photostimulated Regeneration of an Antigen-Sensing Electrode Using a Photoisomerizable Antigen-Monolayer Electrode

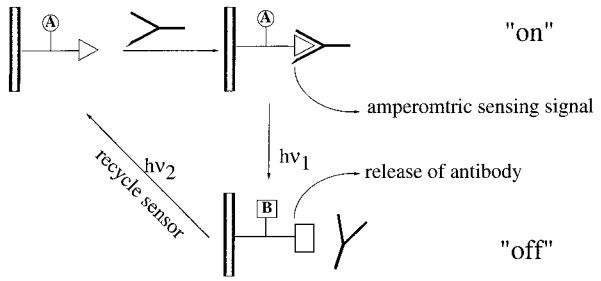

or receptor−protein assemblies at electrode surfaces would perturb the capacitance and resistance of the electrode/electrolyte interface. Thus, impedance could provide a general method to follow the formation or dissociation of antigen−antibody complexes at modified electrode surfaces. Indeed, several reports have addressed the impedance transduction of the affinity complexes between antigens and antibodies[16] or biotin and avidin.[17] Here we wish to report on the application of impedance spectroscopy to probe the photostimulated formation and dissociation of antigen−antibody complexes formed between the DNP-Ab and a photoisomerizable dinitrospiropyran antigen monolayer electrode. The electronic signal following the formation of the antigen−antibody complexes is specifically amplified by the application of Faradaic impedance measurements using a molecular redox probe or biocatalytic reactions. These impedance measurements enable us to tailor analogous resistance capacitance electronic circuits that provide physical insight to the biological interactions at the sensing interface.

Experimental Section

Chemicals. 1-(4-Mercaptobutyl)-3,3-dimethyl-6′,8′-dinitrospiro-[2′*H*-1-benzopyran-2′,2-indoline] (**1a**) was synthesized according to the published procedure.[18] Dinitrophenyl antibody, DNP-antibody, **2** (monoclonal mouse IgE anti-DNP, Sigma), was used as supplied. Glucose oxidase, GOx (EC. 1.1.3.4, from *Aspergilus niger*), covalently modified with tethered ferrocene units, GOx−Fc (**3**), was prepared by the reaction of GOx with *N*-(2-methylferrocene)caproic acid, (**4**) in the presence of 1-ethyl-3-(3-(dimethylamino)propyl)carbodiimide, EDC, and purified according to the published procedure.[19] All other chemicals (Aldrich or Sigma) were used as supplied without further purification. Ultrapure water from a Nanopure (Barnstead) source was used throughout this work.

Electrode Modification. Au-disk electrodes (diameter 1.6 mm, geometrical area ca. 0.02 cm^2) embedded into Teflon holders were polished with silicon carbide P4000 grinding paper (Buehler) on a "ECOMET3" (Buehler) motorized wheel using a polishing cloth (Buehler) with wet alumina powder of finer and finer grades (from 1 μm down to 0.05 μm). The polished electrodes were rinsed twice with water, each time for 5 min, using an ultrasonic bath and cycled from −0.5 to 1.4 V vs Ag/AgCl in 0.01 M $HClO_4$ at 50 mV s^{-1} until a stable background current was obtained (normally 50 cycles). The real area of the electrode surface, taking a roughness factor, ca. 2.3, into account, was found[20] to be ca. 0.046 cm^2. Electrode modification was conducted by dipping the electrodes in 20 mM thiolated dinitrospiropyran **(1a)** ethanolic solution for 12 h. The modified electrodes were rinsed with pure ethanol and water. To generate the dinitrospiropyran monolayer state (**1a**), the electrode was irradiated for 3 min with visible light, $\lambda > 495$ nm, using a 150 W xenon lamp (Oriel). To generate the protonated dinitromerocyanine monolayer state (**1b**), the electrode was illuminated for 3 min with UV light, using a Hg-pencil lamp (Oriel 6042) light source and an appropriate filter, 360 nm $< \lambda <$ 380 nm.[11,12] The experiment was performed in a semi-dark room to keep the respective monolayer states. The **1a**- or **1b**-monolayer-modified electrodes were incubated (if required) in 0.1 mg mL^{-1} DNP-Ab solution in 0.1 M phosphate buffer, pH 7.0, at 35 °C for 10 min and then rinsed with the pure phosphate buffer. To dissociate the antigen−antibody complex on the electrode surface, the electrode was irradiated, 360 nm $< \lambda <$ 380 nm, for 10 min and rinsed with 0.1 M phosphate buffer, pH 7.0.

Electrochemical Measurements. A conventional three-electrode cell comprising the antigen- or antigen−antibody-monolayer-modified Au-disk electrode as the working electrode, a large surface Pt electrode as the counter electrode, and a Ag/AgCl-saturated electrode as the reference electrode was used for the impedance measurements. The working electrode was subjected to appropriate irradiation and DNP-Ab treatment (when required) prior to the impedance measurements. The cell was enclosed in a grounded Faraday cage. Impedance measurements were performed using electrochemical impedance analyzer (model 6310, EG&G) connected to a computer (EG&G 398 software) at 25 ± 2 °C. Non-Faradaic impedance measurements were performed in 0.01 M phosphate buffer, pH 7.0, as a background electrolyte. Faradaic impedance measurements were performed in the presence of 10 mM $K_3[Fe(CN)_6]/K_4[Fe(CN)_6]$, 1:1 mixture, as a redox probe or in the presence of a bioelectrocatalytic system comprising 3 mg mL^{-1} GOx−Fc (**3**) and 100 mM glucose in the same background electrolyte. The electrode capacitance was calculated for the real electrode area taking the electrode roughness factor into account. Faradaic impedance spectra are plotted in the form of complex plane diagrams (Nyquist plots). The experimental data were analyzed by the Kramers-Kroenig procedure to confirm true frequency-dependence impedance. For this purpose, commercial software (Boukamp, B. A. Equivalent Circuit (EQUIVCRT.PAS), version 4.5; Universiteit Twente) was employed and the calculated impedance data were found to fit the experimental results.

Results and Discussions

Theoretical Background. The assembly of the dinitrospiropyran thiol (**1a**) monolayer on the Au-electrode surface, its reversible photochemical transformation into the protonated dinitromerocyanine state **(1b)** and back to the spiropyran state (**1a**), as well as the association of the dinitrophenyl antibody, DNP-Ab to the **1a** monolayer interface are schematically presented in Scheme 2. Previous electrochemical and quartz-crystal-microbalance[11,12] experiments revealed that the surface coverage of the thiolated dinitrospiropyran monolayer is ca. 5 × 10^{-11} mol cm^{-2}. Impedance spectroscopy[14] offers an excellent method to probe the photoisomerization of the monolayer associated with the electrode and to follow the antibody binding or dissociation to or from the photoisomerizable monolayer, respectively. By extracting equivalent circuits, we can model chemical transformations occurring at the monolayer interface. A small-amplitude sinusoidal voltage signal is applied to the electrochemical cell, and the resulting current response is measured. The impedance is calculated as the ratio between the system voltage phasor, $U(j\omega)$, and the current phasor, $I(j\omega)$, which are generated by a frequency response analyzer during the experiment, eq 1, where $j = \sqrt{-1}$ and ω and f (excitation frequency) have units of rad s^{-1} and Hz, respectively; $\omega = 2\pi f$.

$$Z(j\omega) = U(j\omega)/I(j\omega) = Z_{re}(\omega) + jZ_{im}(\omega) \qquad (1)$$

SCHEME 2: Assembly of the Photoisomerizable Dinitrospiropyran Monolayer onto a Au Electrode and Its Interaction with the DNP-Ab

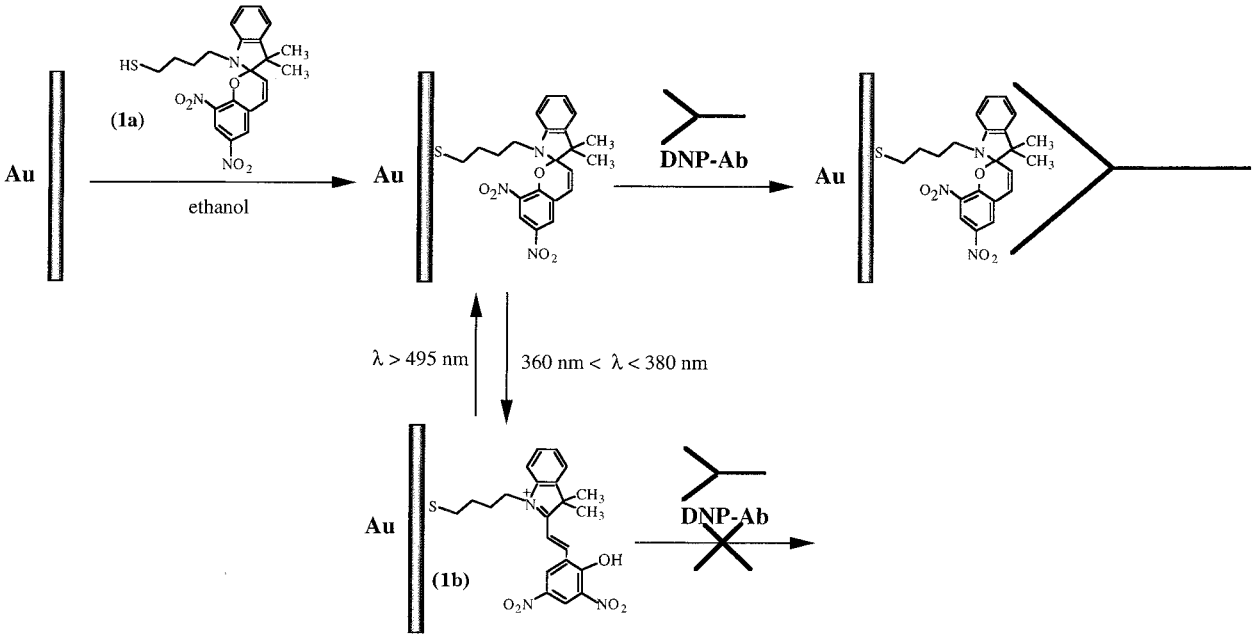

The complex impedance can be presented as a sum of real, $Z_{re}(\omega)$, and imaginary, $Z_{im}(\omega)$ components that are mainly contributed to by the resistance and capacitance of the cell, respectively. The general electronic equivalent scheme (Randles and Ershler model[21]) includes ohmic resistance of the electrolyte solution, R_s, Warburg impedance, Z_w, resulting from the diffusion of ions to the interface from the bulk of the electrolyte, double-layer capacitance, C_{dl}, and electron-transfer resistance, R_{et}, that exists if a redox probe is applied, Scheme 3A. The parallel elements (C_{dl} and $Z_w + R_{et}$) of the equivalent circuit are introduced since the total current through the working interface is the sum of distinct contributions from the Faradaic process, i_f, and double-layer charging, i_c. All the current must pass through the uncompensated resistance of the electrolyte solution, and therefore, R_s is inserted as a series element in the circuit. The two components of the scheme, R_s and Z_w, represent bulk properties of the electrolyte solution and diffusion of the applied redox probe, thus, they are not affected by chemical transformations occurring at the electrode interface. The other two components of the scheme, C_{dl} and R_{et}, depend on the dielectric and insulating features at the electrode/electrolyte interface. Photoinduced isomerization of the monolayer between neutral and charged states and the association and dissociation of DNP-Ab to and from the monolayer are anticipated to result in variation of interfacial properties of the electrode. To introduce these variations into the equivalent scheme, the double-layer capacitance, C_{dl}, and the electron-transfer resistance, R_{et}, are represented as a combination of constant and variable components. The double-layer capacitance consists of the constant capacitance of an unmodified Au-electrode surface, C_{Au} (ca. 40−60 μF cm^{-2} for a polycrystalline gold electrode depending on the applied potential[22]), and the variable capacitance introduced by the surface modifier, C_{mod}, Scheme 3B. Any modifier introduced into the double-charged layer decreases the capacitance in comparison with a pure Au surface.[14] Thus, the combination of C_{Au} and C_{mod} should be presented as a series and the whole double-layer capacitance can be calculated according to eq 2.

The electron-transfer resistance, R_{et}, depends on the electron-transfer kinetics of the introduced redox probe, and it is expected

SCHEME 3[a]

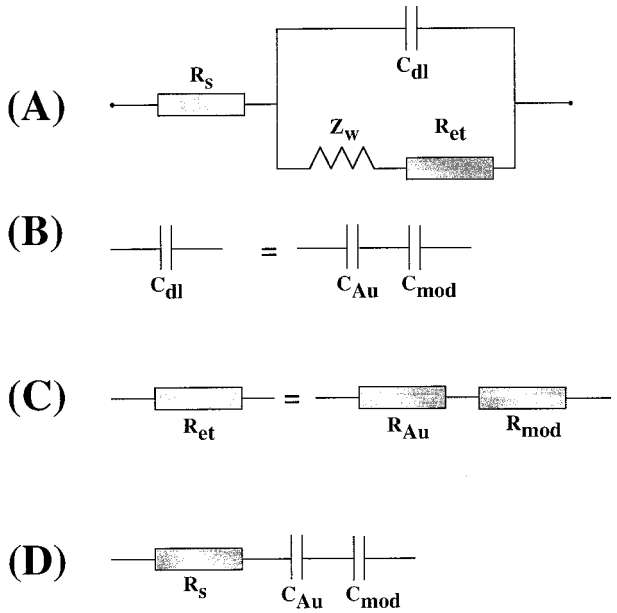

[a] (A) General equivalent circuit for the impedance spectroscopy measurements. (B) Equivalent circuit corresponding to the double-layer capacitance that includes the variable modifier component, C_{mod}, depending on the monolayer state. (C) Equivalent circuit for the electron-transfer resistance that includes the variable modifier component, R_{mod}, corresponding to the different monolayer states. (D) Equivalent circuit for the non-Faradaic impedance measurements in the absence of the redox probe.

$$\frac{1}{C_{dl}} = \frac{1}{C_{Au}} + \frac{1}{C_{mod}} \qquad (2)$$

to be retarded by any inert component existing on the interface and creating a barrier for the electrochemical process. Thus, the whole electron-transfer resistance can be schematically presented as a sequence of two resistances, Scheme 3C, where R_{Au} is the electron-transfer resistance of an unmodified Au-electrode constant for the selected redox probe and R_{mod} corresponds to the additional variable resistance for the electron-

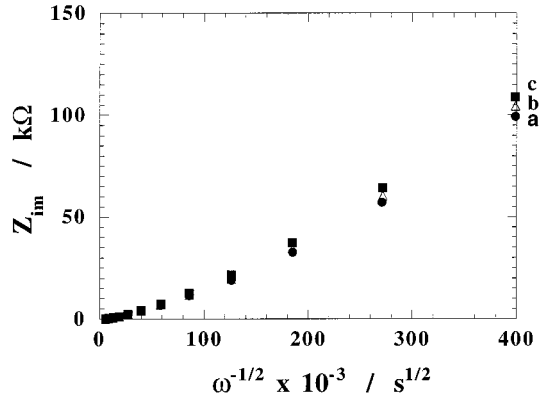

Figure 1. Diagram Z_{im} vs $\omega^{-1/2}$ for the non-Faradaic impedance measurements at the **1a**/**1b**-monolayer-modified Au electrode: (a) **1b**-monolayer state, (b) **1a**-monolayer state, (c) affinity complex of DNP-Ab with the **1a**-monolayer. Applied bias constant potential, 0.6 V; amplitude of the alternating voltage, 10 mV; the background electrolyte was composed of 0.01 M phosphate buffer, pH 7.0.

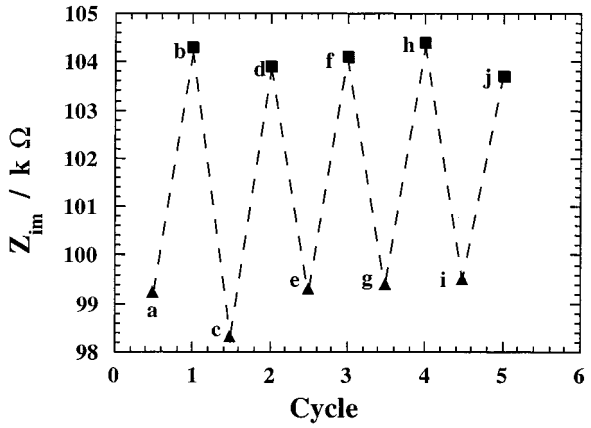

Figure 2. Reversible change of the imaginary part of the impedance, Z_{im}, upon cyclic photoisomerization of the monolayer between the **1a**/**1b**-monolayer states: (b, d, f, h, and j) **1a** state; a, c, e, g, and i) **1b** state. Measurements were performed applying the constant bias potential, 0.6 V; amplitude of the alternating voltage, 10 mV; in the absence of the redox probe and antibodies. The Z_{im} values were measured at $f = 1$ Hz.

transfer process introduced by the modifier. The total resistance, R_{et}, can be expressed by eq 3.

$$R_{et} = R_{Au} + R_{mod} \tag{3}$$

Analysis of $Z_{re}(\omega)$ and $Z_{im}(\omega)$ developed at different frequencies allows the calculation of the following important parameters: (a) the double-layer capacitance, C_{dl}, and its variable component, C_{mod}, (b) the electron-transfer rate constant for the applied redox probe derived from the electron-transfer resistance, R_{et}, and its variable component, R_{mod}. In the absence of any redox probe in the electrolyte solution, only non-Faradaic impedance is operative. The electron-transfer characterizing parameters, R_{et} and Z_w, became infinite, and the equivalent circuit can be simplified, as shown in Scheme 3D. The variable component in the circuit is presented by C_{mod}, and it affects the imaginary part of the impedance, Z_{im}, eq 4.

$$Z_{im} = \frac{1}{\omega C_{dl}} \tag{4}$$

Equation 4 was evaluated considering only the dense part of the double-charged layer.

The experimental results can be analyzed graphically[14] (usually in Nyquist coordinates: Z_{im} vs Z_{re}) in the frame of the theoretical model.[21] All electronic characteristics of the equivalent circuit and the corresponding physical parameters of the real electrochemical system can be extracted from such analysis. Since the variable parameters of the system are the functions of the monolayer state and composition, they can be used to quantitatively characterize the monolayer.

Impedance of the Photoisomerizable Monolayer Electrode in the Absence of a Redox Probe. In the absence of a redox probe and, thus, without a Faradaic current, the system can be considered as an ideally polarized electrode (equivalent circuit shown in Scheme 3D).[14] The experimental results obtained for the **1a**- and **1b**-monolayer-modified Au electrode plotted in Nyquist coordinates Z_{im} vs Z_{re} represent almost identical straight lines perpendicular to the Z_{re} axis intersecting the axis at $Z_{re} = R_s$ (not shown). Since the **1a**- and **1b**-monolayer-modified electrodes differ only by their double-layer capacitance, C_{dl}, and thus by Z_{im} (cf. eq 4), the experimental results are plotted in the coordinates Z_{im} vs $\omega^{-1/2}$, Figure 1 (curve a and b). The data present almost linear dependencies slightly deviating at high frequency, in accordance with eq 4. It is evident that Z_{im} of the **1a**-monolayer-modified electrode is higher than Z_{im} of the **1b** state of the electrode. This implies that the capacitance of the noncharged dinitrospiropyran monolayer is lower than the capacitance of the positively charged protonated dinitromerocyanine monolayer. This result agrees with usual electrochemical behavior of molecules exhibiting different polarities and adsorbed onto electrodes.[14] The capacitance depends on the dielectric permittivity introduced into the double-charged layer molecules ($\epsilon_{dl} = \epsilon_0\epsilon_\rho$), and for the less polar molecules, the capacitance should be smaller, eq 5, where ϵ_0 is the permittivity of free space, ϵ_ρ is the effective dielectric constant of the layer separating the ionic charges and the electrode surface, A is the electrode area (cm^2), and d is the thickness of the separating layer.

$$C_{dl} = (\epsilon_0\epsilon_\rho A)/d \tag{5}$$

The experimentally observed double-layer capacitance of the modified electrode was 15.1 and 16.4 μF cm^{-2} for the **1a** and **1b** states, respectively. The variable component of the capacitance depending on the modifier isomer state, C_{mod}, was extracted from the total interfacial capacitance, C_{dl}, using eq 2. The values 21.6 and 24.4 μF cm^{-2} for the **1a** and **1b** states were derived, respectively. It should be noted that Z_{im} and the corresponding C_{dl} of both isomer states of the functionalized electrodes differ substantially from the respective parameters characterizing the bare Au electrodes but much less than in the case of densely packed long alkyl thiol monolayers.[23] This suggests that the **1a** and **1b** monolayers are not densely packed assemblies. Defects in the monolayer structures resulting in pinholes yield a lower contribution to the variable modifier capacitance, C_{mod}, compared to a densely-packed long alkyl-chain thiol modifier. The small difference between Z_{im} of the **1a** and **1b** monolayers is, however, well reproducible and can be repeatedly observed upon cyclic photoisomerization of the monolayer between the dinitrospiropyran (**1a**) and protonated dinitromerocyanine (**1b**) states, Figure 2. Thus, the photonic signals that activate the photoisomerization of the monolayer can be transduced by the impedance responses of the monolayer electrode in its two states. Association of the dinitrophenyl antibody, DNP-Ab, to the dinitrospiropyran monolayer (Scheme 2) is expected to yield a thick hydrophobic layer on the electrode surface. Earlier microgravimetric, quartz-crystal-microbalance

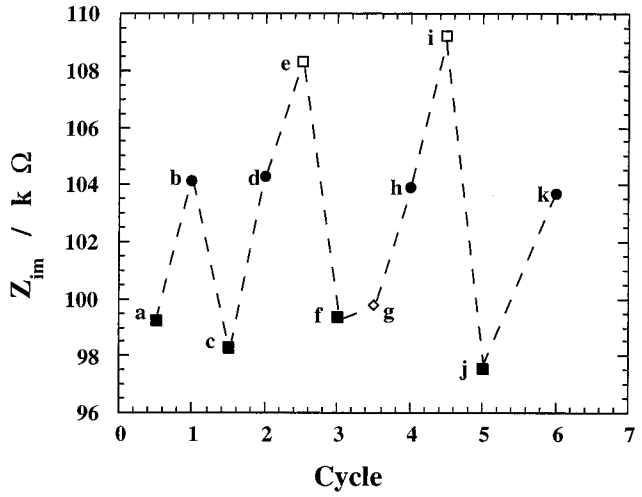

Figure 3. Cyclic changes of the imaginary part of the impedance, Z_{im}, upon photoisomerization of the monolayer between the **1a**/**1b** states and upon introduction of DNP-Ab or its dissociation from the monolayer electrode: (a and c) monolayer in **1b** state; (b and d) monolayer in **1a**-state; (e) monolayer in **1a**-state upon addition of DNP-Ab; (f) **1b**-monolayer after washing off the DNP-Ab; (g) Readdition of DNP-Ab to **1b**-monolayer state; (h) washing off the antibody followed by photoisomerization of the monolayer to state **1a**; (i) Addition of DNP-Ab to the **1a** monolayer state; (j) photoisomerization of the monolayer to the **1b**-state followed by rinsing off the antibody; (k) photoisomerization of the monolayer to the **1a**-state. For all systems, Z_{im} was measured at $f = 1$ Hz.

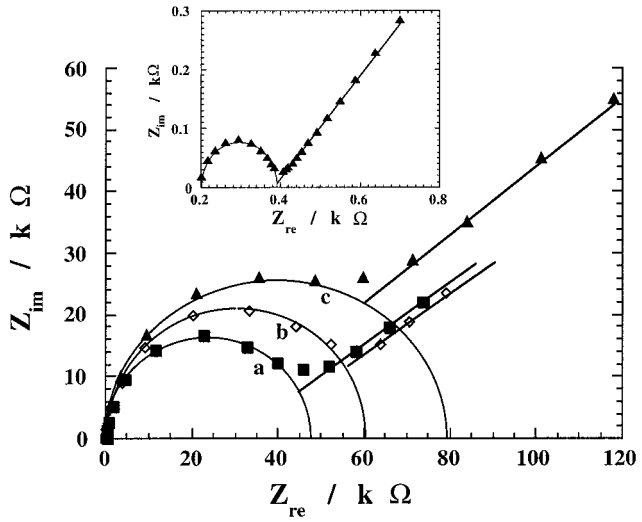

Figure 4. Nyquist diagram (Z_{im} vs Z_{re}) for the Faradaic impedance measurements at the **1a**/**1b**-monolayer-modified Au electrode in the presence of 10 mM $[Fe(CN)_6]^{3-/4-}$: (a) **1b**-monolayer state, (b) **1a**-monolayer state, (c) affinity complex of DNP-Ab with the **1a**-monolayer. Applied bias constant potential, 0.6 V; amplitude of the alternating voltage, 10 mV; composition of the background electrolyte, 0.01 M phosphate buffer, pH 7.0. Impedance measurements were performed in the frequency range of from 10 mHz to 20 kHz. Inset: Impedance response at a bare Au electrode.

experiments[12] indicated that the saturated surface coverage of DNP-Ab on the dinitrospiropyran monolayer is 4×10^{-12} mol cm^{-2}. Thus, ca. 10% of the monolayer antigen sites are associated to DNP-Ab. Thus, an additional capacitance component should be introduced into the system, resulting in a further decrease in the overall double-layer capacitance, C_{dl}, according to eq 2. Figure 1 (curve c) shows the observed impedance, Z_{im}, of the dinitrospiropyran (**1a**) monolayer electrode in the presence of DNP-Ab. A slight increase in the Z_{im} values is observed as compared to the antibody untreated **1a**-functionalized electrode. This is consistant with the fact that the DNP-Ab association to the monolayer adds an additional capacitance value to the overall variable modifier capacitance. As a result, the overall double-layer capacitance decreases and the observed Z_{im} increases (cf. eq 4). The variable component, C_{mod}, corresponding to the surface complex of DNP-Ab with the **1a** monolayer (19.8 μF cm^{-2}) is smaller than the respective value of **1a** monolayer in the absence of the antibody. Upon photoisomerization of the dinitrospiropyran to the protonated merocyanine state (**1b**), the monolayer lacks the affinity to DNP-Ab and can be washed off from the monolayer. In this case, the impedance returns back to the value characteristic for the **1b** state, Figure 1, curve a. This reversible change of the impedance can be repeatedly observed upon application of the corresponding irradiation steps and antibody addition/washing steps (Figure 3). Addition of DNP-Ab to the (**1b**) monolayer electrode does not affect its impedance, since the antibodies do not produce a surface-associated affinity complex with the **1b** monolayer.

Impedance of the Photoisomerizable Monolayer Electrode in the Presence of a Redox Probe. Faradaic current and the corresponding real component of the impedance, Z_{re}, observed in the presence of a redox probe can significantly contribute to the resulting impedance spectrum. The equivalent circuit, in the presence of a redox probe solubilized in the electrolyte, should include all the components shown in Scheme 3A. Figure 4 shows the impedance features, presented as Nyquist plots (Z_{im} vs Z_{re}) of the dinitrospiropyran (**1a**) and protonated dinitromerocyanine (**1b**) electrodes in the presence of $[Fe(CN)_6]^{3-/4-}$ as redox probe. A significant difference between the impedance spectra of the **1b** and **1a** monolayer-modified electrodes is observed (Figure 4, curves a and b, respectively). This difference is substantially higher than the impedance spectra difference observed in the absence of the redox probe. The observed impedance spectra follow the theoretically expected shape[14] and include a semicircle lying on the Z_{re} axis continued with a straight line. The semicircle portion observed at the higher frequencies corresponds to the electron-transfer-limited process, whereas the linear part is characteristic of the lower frequencies and represents the diffusionally limited process. Thus, the electron-transfer kinetic parameters and diffusional characteristics can be extracted from the semicircle and linear parts of the impedance spectra, respectively.[14] The semicircle diameter is equal to the electron transfer resistance, R_{el}. The intercept of the semicircle with the Z_{re} axis at high frequencies ($\omega \rightarrow \infty$) is equal to the electrolyte solution resistance, R_s. Extrapolation of the circle to lower frequencies yields an intercept corresponding to $R_s + R_{el}$. The maximum value of the imaginary impedance in the semicircle part corresponds to $Z_{im} = R_{et}/2$ and is achieved at the characteristic frequency, ω_0, eq 6. The characteristic frequency has the meaning of the

$$\omega_0 = (C_{dl}R_{et})^{-1} \tag{6}$$

inverted time constant of the equivalent circuit, τ, eq 7.

$$\tau = (\omega_0)^{-1} \tag{7}$$

The electron-transfer resistance can be translated into the exchange current under equilibrium, I_0, eq 8, and then the heterogeneous electron-transfer, k_{et}, can be evaluated, taking into

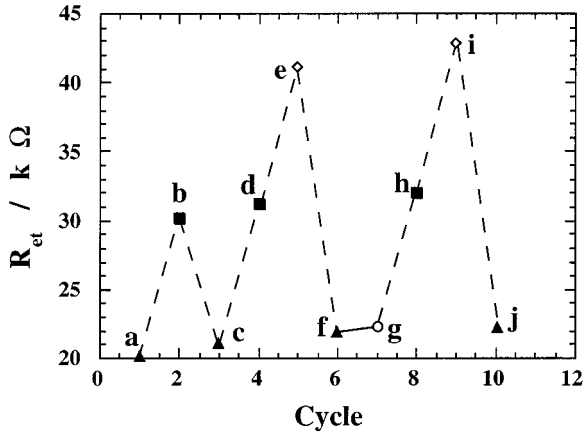

Figure 5. Cyclic change of the electron-transfer resistance, R_{et}, upon photoisomerization of the monolayer between **1a**/**1b** states, and association or dissociation of DNP-Ab to and from the monolayer interface: (a and c) monolayer in **1b**-state; (b and d) monolayer in **1a** state; (e) **1a** monolayer upon addition of DNP-Ab; (f) photoisomerization to **1b**-monolayer state and washing off DNP-Ab; (g) **1b**-monolayer upon addition of DNP-Ab; (h) washing off the DNP-Ab followed by photoisomerization of the monolayer to **1a** state; (i) addition of DNP-Ab to **1a** monolayer; (j) photoisomerization of the monolayer to **1b** state and washing off DNP-Ab. Measurements were performed applying a constant bias potential, 0.6 V; amplitude of alternating voltage, 10 mV, using $[Fe(CN)_6]^{3-/4-}$, 1×10^{-2} M, as the redox probe.

account the dependence of k_{et} on the applied potential,[14] eq 9

$$R_{et} = RT\,(nFI_0)^{-1} \tag{8}$$

$$I_0 = nFAk_{et}[S]\,\exp[-\alpha nF\Delta E/(RT)] \tag{9}$$

where R is the gas constant, T is the temperature (K), A is the electrode area (cm^2), $[S]$ corresponds to the bulk concentration of the redox probe (mol cm^{-3}), n is the number of transferred electrons, α is the electron-transfer coefficient, and ΔE is the applied overpotential.

The experimental impedance spectra show larger R_{et} when the monolayer is in the neutral dinitrospiropyran state (**1a**) in comparison with R_{et} obtained with the positively charged protonated merocyanine state (**1b**) (Figure 4, curves b and a). It should be noted that both of them are much bigger then the R_{et} of the bare Au electrode (Figure 4, inset). The heterogeneous rate constants for the electron transfer between the electrode and the redox probe are calculated according to eqs 8 and 9: 2.7×10^{-3}, 0.82×10^{-5}, 1.1×10^{-5} cm s^{-1} for the bare Au electrode and **1a** and **1b**-monolayer modified Au electrode, respectively. It is evident that both modifier states inhibit the electron-transfer process to the redox probe as compared to the bare Au electrode. The positively charged protonated dinitromerocyanine **1b**-monolayer-functionalized electrode reveals improved interfacial electron-transfer kinetics as compared to the neutral dinitrospiropyran **1a**-monolayer-modified electrode. The enhanced interfacial electron transfer in the presence of the **1b**-monolayer assembly is attributed to the electrostatic attraction and concentration of the negatively charged redox probe at the charged monolayer (Frumkin effect).[24] A similar acceleration of interfacial electron-transfer rates was observed with different modified electrodes and charged redox probes.[25] Cyclic photoisomerization of the monolayer between the **1a** state to the **1b** state results in the reversible change of the impedance spectra and the corresponding electrochemical parameters, Figure 5. With the **1b**-monolayer electrode, low electron-transfer resistance is observed (Figure 5 points a and c, 20 ± 1 kΩ), whereas a high electron-transfer resistance is observed for the **1a**-monolayer electrode (Figure 5, points b and d), 30 ± 2 kΩ).

The fact that the Faradaic impedance spectrum of the **1b**-monolayer electrode after rinsing off DNP-Ab returns to the original spectrum of the **1b**-monolayer electrode and the fact that the impedance spectrum of the **1b**-monolayer electrode is unaffected upon addition of DNP-Ab indicate that the antibody does not bind to the **1b**-monolayer interface by nonspecific interactions. The Faradaic impedance measurements reveal sensitivities to the photoisomer state of the monolayer configuration in the imaginary and real impedance components (Z_{im} or Z_{re}). As a result, Faradaic impedance spectroscopy provides a dual transduction signal for the light-stimulated isomerization of the monolayer assembly (photonic recording process). We also note that the Faradaic impedance spectra of the two photoisomer states of the monolayer electrodes differ substantially as compared to the minor impedance difference observed under non-Faradaic conditions. This can be explained by the fact that non-Faradaic impedance is only sensitive to capacitance changes of the monolayer, whereas the Faradaic impedance spectra are affected by interfacial electron-transfer rates and controlled by electrostatic attractive interactions between the negatively-charged redox probe and the charged monolayer interface. Thus, Faradaic impedance provides a means to amplify the transduced signal reflecting the photoisomerization of the monolayer.

The association of DNP-Ab to the dinitrospiropyran monolayer electrode is expected to be reflected in the Faradaic impedance spectra. Binding of DNP-Ab to the antigen monolayer is anticipated to insulate interfacial electron transfer and thus introduces a barrier for the electron transfer. Figure 4, curve c, shows the Faradaic impedance spectrum of the dinitrospiropyran **1a**-monolayer electrode upon treatment with the DNP-Ab and in the presence of the $[Fe(CN)_6]^{3-/4-}$ redox probe. A substantially larger semicircle is observed as compared to the **1a**-modified monolayer electrode, indicating an increased electron-transfer resistance upon binding DNP-Ab to the monolayer electrode. The derived electron-transfer rate constant to the redox probe is retarded upon binding DNP-Ab to the electrode and corresponds to $k_{et} = 0.58 \times 10^{-5}$ cm s^{-1}. Treatment of the protonated dinitromerocyanine **1b**-monolayer electrode with DNP-Ab does affect the Faradaic impedance spectrum, and a spectrum almost overlapping that shown in Figure 4, curve a, is observed. This is consistant with the fact that DNP-Ab does not bind to the **1b**-monolayer interface. The reversible light-stimulated association and dissociation of DNP-Ab to and from the photoisomerizable monolayer is transduced by Faradaic impedance measurements by the cyclic photoisomerization of the monolayer between **1a** and **1b** states, Figure 5. The electron-transfer resistance of the dinitrospiropyran **1a** monolayer is ca. 30 ± 2 kΩ (Figure 5, point d). Association of DNP-Ab to the **1a** monolayer increases the electron-transfer resistance (42 ± 2 kΩ, Figure 5, point e). Photoisomerization of the monolayer to the dinitrospiropyran **1b**-monolayer state, followed by rinsing of the electrode, decreases substantially the electron transfer resistance (Figure 5, point f). Treatment of the **1b** monolayer with DNP-Ab does not influence the electron-transfer resistance (Figure 5, point g), implying that the antibody does not bind to the **1b**-monolayer electrode. Rinsing off DNP-Ab from the **1b**-monolayer electrode and photoisomerization of the monolayer to the **1a** state restores the characteristic electron-transfer resistance (Figure 5, point h). Addition of the DNP-Ab results in its binding to the antigen monolayer electrode and the increase

SCHEME 4: Schematic Activity of an Optoelectronic Gated Switch Operating between the 1a and 1b Monolayer States

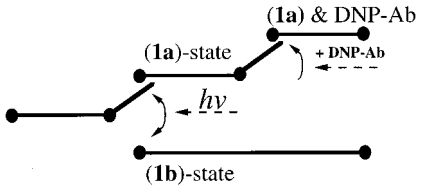

of the electron-transfer resistance, whereas photoisomerization of the monolayer to the **1b** state enables one to wash off the antibody and transduce the binding and dissociation of DNP-Ab to and from the monolayer-functionalized electrode by means of electron-transfer resistance (Figure 5, points i and j, respectively). The Faradaic impedance transduction of the photoisomerization of the monolayer interface and the association/dissociation of DNP-Ab represents a three-positioned optobioelectronic switch consisting of two "OR" gates. The high electron-transfer resistance is only obtained upon photoisomerization of the **1b** monolayer interface to the **1a**-monolayer configuration and upon the association of DNP-Ab to the interface, Scheme 4.

It should be noted that the capacitance is also changed upon photoisomerization of the monolayer and its association with the antibody. The characteristic time constant of the equivalent electronic circuit derived from the double-layer capacitance and the electron-transfer resistance (eqs 6, 7) increases in the following order: 4.0×10^{-4}, 0.11 , 0.23, and 0.49 s for the bare Au electrode, the **1b** monolayer, the **1a** monolayer, and the DNP-Ab/**1a** monolayer complex, respectively.

The variable component of the electron-transfer resistance, R_{mod}, for the electrode surface that includes the DNP-Ab/**1a**-complex depends on the perfection of the monolayer. The R_{mod} is decreased due to the availability of pinholes in the monolayer permitting the penetration of the redox probe to the electrode surface. Application of high molecular-weight biomolecules[26] or redox enzymes[27] as the redox probe was reported to eliminate the permeability of the probe through pinhole monolayer defects. Indeed, the Faradaic currents associated with redox proteins were found to be entirely blocked upon formation of antigen−antibody complexes at electrode supports in a series of cyclic voltammetry experiments.[26,27] Thus, to enhance the Faradaic impedance changes upon formation of the antigen−antibody complex or its dissociation upon photoisomerization of the monolayer, we applied ferrocene-modified glucose oxidase, GOx−Fc, in the presence of glucose as the redox-active protein probe. Glucose oxidase by itself does not electrically communicate with the electrode support. Tethering of ferrocene units to the protein shorten the electron-transfer distances between the enzyme redox center and the electrode, enabling mediated electron transfer.[28] The resulting electrically contacted glucose oxidase stimulates the bioelectrocatalyzed oxidation of glucose. Thus, association of DNP-Ab to the dinitrospiropyran **1a**-monolayer electrode is anticipated to introduce a high electron-transfer resistance that blocks the bioelectrocatalytic features of GOx−Fc.

Figure 6 (curves a and b) shows the Nyquist diagram (Z_{im} vs Z_{re}) for Faradaic impedance measured at the **1a**/**1b**-monolayer-modified Au electrode in the presence of biocatalytic system, GOx−Fc and glucose, as the redox probe. The impedance spectra show the typical patterns consisting of large semicircles and the initiation of the linear parts, characteristic of the kinetically and diffusionally limited processes, respectively. The

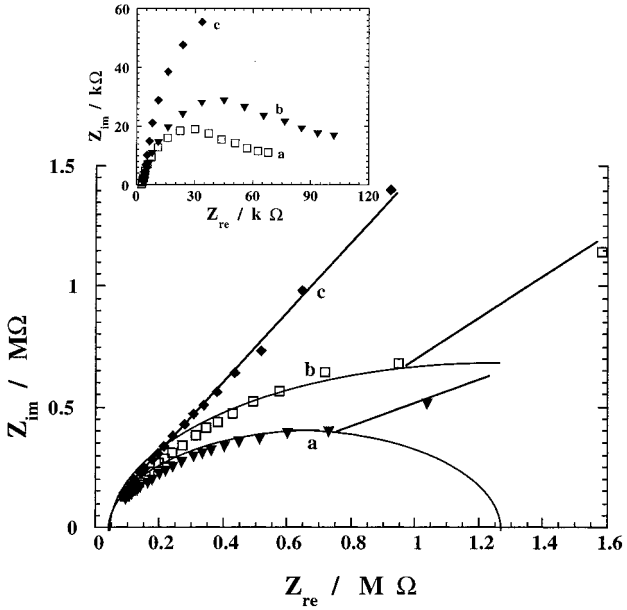

Figure 6. Nyquist diagram (Z_{im} vs Z_{re}) for the Faradaic impedance measurements at the **1a**/**1b**-monolayer-modified Au electrode in the presence of GOx−Fc, 3 mg mL^{-1} and glucose, 1×10^{-1} M: (a) **1b**-monolayer state, (b) **1a**-monolayer state, (c) affinity complex of DNP-Ab with the **1a**-monolayer. Applied bias constant potential, 0.4 V; amplitude of the alternating voltage, 10 mV; the background electrolyte, 0.01 M phosphate buffer, pH 7.0. Impedance measurements were performed in the frequency range of from 10 mHz to 20 kHz. Inset: Nyquist-diagram in the high-frequency region: (a−c) the same as in the main plot.

semicircle and the derived electron-transfer resistance are smaller in the case of **1b** monolayer than **1a** monolayer (Figure 6, curve a and b, respectively). This results from the association of the negatively charged (at pH 7.0) glucose oxidase molecules (isoelectric point, pI = 4)[29] with the positively charged protonated (pK = 8.6)[30] dinitromerocyanine monolayer (**1b**). The electrostatic attraction of the redox enzyme to the positively charged monolayer interface enhances the electron-transfer process, resulting in a smaller R_{et} value. It should be mentioned that at the bare Au electrode, a smaller semicircle and R_{et} (not shown) than that observed with the positively charged **1b**-monolayer-modified electrode is obtained. Thus, any modifier associated with the electrodes creates an additional barrier for electron transfer to the biocatalytic redox probe, and this is shown in the equivalent circuit (Scheme 3A) as the variable part of the electron-transfer resistance, R_{mod}. In fact, previous cyclic voltammetry experiments[10] have identified the photoswitchable activation/deactivation of GOx−Fc in the presence of the photoswitchable dinitrospiropyran monolayer electrode. The high electron-transfer resistance observed with the dinitrospiropyran **1a**-monolayer configuration nicely explains the switched-off biocatalytic state in the amperometric experiments.

Association of DNP-Ab with the **1a**-monolayer electrode results in a dramatic increase of the semicircle that looks like a straight line, Figure 6, curve c. The corresponding R_{et} is so high that it cannot be evaluated from the plot. This tremendous increase of the R_{et} value upon association of DNP-Ab results from impermeability of the antibody monolayer for the GOx−Fc molecules. Photoisomerization of the dinitrospiropyran−DNP-Ab monolayer to the protonated dinitromerocyanine (**1b**) monolayer state enables the dissociation of the antibody and the regeneration of the active **1a** antigen monolayer for binding DNP-Ab is achieved by photoisomerization of the **1b** monolayer electrode to the **1a**-monolayer state, Figure 7. Binding of DNP-

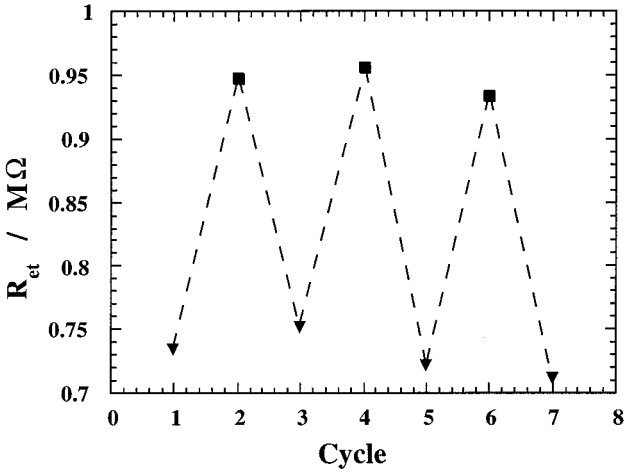

Figure 7. Cyclic change of the electron-transfer resistance, R_{et}, upon photochemically induced transformation of **1a**/**1b** monolayer: (▼) **1b**, (■) **1a**. Measurements were performed applying the constant bias potential, 0.4 V; amplitude of the alternating voltage, 10 mV; in the presence of GOx−Fc, 3 mg mL^{-1}, glucose, 1×10^{-1} M.

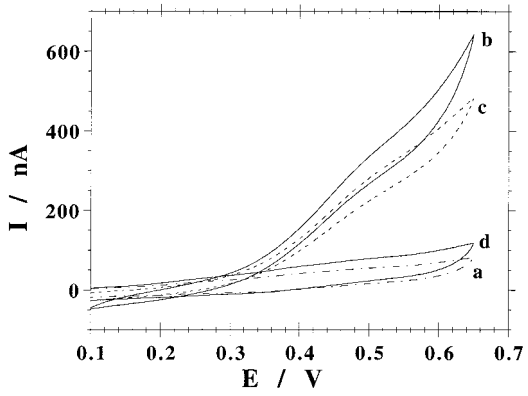

Figure 8. Cyclic voltammograms of the photoisomerizable monolayer electrode: (a) background electrolyte solution and electrode in the **1a**-monolayer state; (b) **1b**-monolayer state in the presence of GOx−Fc, 3 mg mL^{-1}, and glucose, 1×10^{-1} M; (c) **1a** monolayer state with added GOx−Fc, 3 mg mL^{-1}, and glucose, 1×10^{-1} M; (d) **1a**-monolayer configuration after treatment with DNP-Ab, in the presence of GOx−Fc, 3 mg mL^{-1}, and glucose, 1×10^{-1} M. All data were recorded under argon in a 0.01 M phosphate buffer solution, pH = 7.0. Scan rate = 2 mV s^{-1}.

Ab to the **1a**-monolayer electrode results in a large semicircle Faradaic impedance corresponding to an electron-transfer resistance of R_{et} = ca. 2 MΩ. Photoisomerization of the monolayer to the protonated merocyanine (**1b**) followed by rinsing of the electrode results in the impedance spectrum characteristic to the **1b**-monolayer electrode, R_{et} = ca. 1.2 MΩ. Further isomerization of the **1b**-monolayer to the **1a**-monolayer state restores its impedance spectrum observed in the absence of the DNP-Ab. Upon challenging the **1a**-monolayer electrode, the impedance spectrum of the **1a**/DNP-Ab complex monolayer characterized by the high electron-transfer resistance is observed. The Faradaic impedance measurements, using GOx−Fc and glucose as the biocatalytic redox probe, enables the electronic transduction of association of DNP-Ab to the **1a**-antigen monolayer and the subsequent photostimulated dissociation of the DNP-Ab from the interface, as well as the light-induced regeneration of the antibody sensing layer. It should be noted that electrochemical regeneration of the enzyme redox center by the biocatalyzed oxidation of glucose provides a means to amplify the electron-transfer reactions at the electrode interface under all limited conditions of electron-transfer resistance of the system in its different states. In addition to the amplification of the electron-transfer events at the electrode interface using GOx−Fc/glucose as the bioelectrocatalytic redox probe, the application of the high molecular-weight enzyme as a redox label for the interfacial electron transfer is advantageous as the electrobiocatalyst is insensitive to pinhole defects in the antigen monolayer array. Careful measurements and examination of the impedance in the high-frequency region reveal additional small semicircles[31] corresponding to the direct electron-transfer process of the ferrocene groups covalently linked to the enzyme molecules, Figure 6 (inset). This primary redox process is responsible for the secondary mediated biocatalytic reaction, and it exhibits a much smaller electron-transfer resistance, R_{et}, and characteristic time, τ. The secondary enzymatic reaction has significantly slower kinetics, and thus, the large semicircle impedance response as a result of the biocatalytic redox reaction represents an amplified output with respect to the primary redox process. It should be noted that in the absence of glucose, the system comprising only GOx−Fc could not realize the biocatalytic process and the respective semicircle but the primary electron-transfer process of the ferrocene groups is still possible. It should be noted that for the small semicircles observed with the **1a**- or **1b**-monolayer electrodes and GOx−Fc in the absence of glucose, the semicircle for the **1a** monolayer is larger than that for the **1b**-monolayer electrode, implying a higher electron-transfer resistance for the dinitrospiropyran monolayer electrode. This is consistant with the electrostatic attraction of GOx−Fc to the **1b**-monolayer electrode that enhances the interfacial electron transfer. Thus, in the absence of glucose, the small primary semicircles were observed but a straight-line characteristic of the non-Faradaic impedance was detected instead of the big semicircles corresponding to the biocatalytic process (not shown). Stepwise increase in the glucose concentration in the presence of the GOx−Fc results in the set of the impedance spectra transforming from the straight line to the typical semicircle.

Further support for the photostimulated control of electron transfer between GOx−Fc and the electrode and for the barrier for electron transfer between the biocatalyst and the electrode upon association of DNP-Ab to the **1a**-monolayer electrode is obtained from cyclic voltammetry experiments, Figure 8. In the presence of the **1b**-monolayer electrode and GOx−Fc/glucose, an electrocatalytic anodic current is observed, Figure 8, curve b, whereas in the presence of the **1a**-monolayer electrode, the bioelectrocatalyzed oxidation of glucose is partly inhibited, Figure 8, curve c. These results imply that the interfacial electron transfer between GOx−Fc and the electrode is facilitated as a result of the electrostatic attraction of the biocatalyst to the positively charged **1b**-monolayer electrode. In the presence of the **1a**-monolayer electrode and upon addition of DNP-Ab, the bioelectrocatalyzed oxidation of glucose is almost entirely blocked, Figure 8, curve d. The cyclic voltammogram of the system is almost identical to the background current of the electrolyte solution in the absence of the GOx−Fc/glucose bioelectrocatalytic redox probe. Thus, association of DNP-Ab to the **1a**-monolayer electrode assembly hinders the interfacial electron transfer and blocks the bioelectrocatalyzed oxidation of glucose.

Conclusions

Impedance spectroscopy was applied to transduce electronically light-induced changes in a photoisomerizable dinitrospiropyran monolayer associated with an electrode. Impedance spectroscopy enabled us to probe the photoisomerization process

of the monolayer array, and as the monolayer exhibits photoswitchable antigen properties for the dinitrophenyl antibody, DNP-Ab, the method enabled us to follow the binding of the antibody to antigen monolayer and its dissociation from the electrode interface. We demonstrated that Faradaic impedance measurements, including the Z_{im} and Z_{re} components, allow the amplification of the transduced signals as compared to non-Faradaic impedance, which is only sensitive to capacity changes. The Faradaic impedance analyses were performed in the presence of a molecular redox probe, e.g., $[Fe(CN)_6]^{3-/4-}$, and in the presence of the macromolecular bioelectrocatalytic system consisting of ferrocene-tethered glucose oxidase, GOx−Fc, acting as an electrically contacted enzyme, and glucose. The advantages of using the bioelectrocatalytic GOx−Fc/glucose system as a redox probe for the interfacial electron transfer at the monolayer electrode include: (i) The bioelectrocatalytic system enables amplification of differences in the electron-transfer behavior at the monolayer interface due to the turnover of the enzyme. (ii) The electron-transfer between the high molecular-weight GOx−Fc and the electrode is insensitive to molecular defects in the monolayer structure, and hence, pure chemical events occurring at the monolayer−electrolyte interface are transduced by the biomolecular redox probe. The study has addressed the application of impedance spectroscopy to probe the binding interactions of the dinitrophenyl antibody, DNP-Ab, with the photoswitchable dinitrospiropyran antigen monolayer electrode. In the dinitrospiropyran (**1a**) monolayer state, DNP-Ab binds to the antigen monolayer, a process that is reflected by enhanced electron-transfer resistance. In the protonated dinitromerocyanine state, DNP-Ab is dissociated from the monolayer interface and electron transfer is facilitated. Impedance spectroscopy nicely complements previous cyclic voltammetry and quartz crystal microbalance (QCM) experiments in probing the photoswitchable interactions of an antibody with a photoisomerizable monolayer and the development of reusable immunosensor electrodes. The advantages of impedance spectroscopy rest on the possibility to translate chemical events occurring at the electrode interface in terms of electronic resistance/capacitance parameters. Finally, the impedance probing of the photoisomerizable monolayer in the absence or in the presence of the DNP-Ab established a gated "OR" optoelectronic switch, Scheme 4. Photoisomerization of the monolayer between the dinitrospiropyran **1a**-monolayer configuration and the protonated dinitromerocyanine **1b**-monolayer structure switch the assembly between two states exhibiting high and low electron-transfer resistances, respectively. The **1a**-monolayer state can be further switched between a low electron-transfer resistance for antigen monolayer electrode and a high electron-transfer resistance obtained upon binding of DNP-Ab to the monolayer assembly.

Acknowledgment. This research was supported by The Israel Science Foundation founded by The Israel Academy of Sciences and Humanities.

References and Notes

(1) (a) Schmidt, H.-L.; Schuhmann, W. *Biosens. Bioelectron.* **1996**, *11*, 127. (b) Bartlett, P. N. In *Biosensor Technology. Fundamentals and Applications*; Buck, R. P., Hatfield, W. E., Umana, M.; Bowden, E. F., Eds.; Marcel Dekker: New York, 1990, Chapter 7, 95−115.

(2) (a) Willner, I.; Katz, E.; Willner, B. *Electroanalysis* **1997**, *13*, 965. (b) Katz, E.; Heleg-Shabtai, V.; Willner, B.; Willner, I.; Bückmann, A. F. *Bioelectrochem. Bioenerg.* **1997**, *42*, 95.

(3) (a) Skladal, P. *Electroanalysis* **1997**, *9*, 737. (b) Ghindilis, A. L.; Atanasov, P.; Wilkins, M.; Wilkins, E. *Biosens. Bioelectron.* **1998**, *13*, 113.

(4) (a) Göpel, W.; Heiduschka, P. *Biosens. Bioelectron.* **1994**, *9*, iii. (b) Willner, I.; Katz, E.; Willner, B.; Blonder, R.; Heleg-Shabtai, V.; Bückmann, A. F. *Biosens. Bioelectron.* **1997**, *12*, 337.

(5) (a) Katz, E.; Willner, B.; Willner, I. *Biosens. Bioelectron.* **1997**, *12*, 703. (b) Willner, I.; Katz, E.; Willner, B.; Blonder, R.; Heleg-Shabtai, V.; Bückmann, A. F. *Biosens. Bioelectron.* **1997**, *12*, 337.

(6) (a) Gilat, S. L.; Kawai, S. H.; Lehn, J.-M. *Chem. Eur. J* **1995**, *1*, 275. (b) Tsivgoulis, G. M.; Lehn, J.-M. *Chem. Eur. J.* **1996**, *2*, 1399.

(7) (a) Lion-Dagan, M.; Katz, E.; Willner, I. *J Am. Chem. Soc.* **1994**, *116*, 7913. (b) Willner, I.; Lion-Dagan, M.; Marx-Tibbon, S.; Katz, E. *J. Am. Chem. Soc.* **1995**, *117*, 6581.

(8) (a) Willner, I.; Blonder, R.; Katz, E.; Stocker, A.; Bückmann, A. F. *J. Am. Chem. Soc.* **1996**, *118*, 5310. (b) Blonder, R.; Katz, E.; Willner, I.; Wray, V.; Bückmann, A. F. *J. Am. Chem. Soc.* **1997**, *119*, 11747.

(9) Lion-Dagan, M.; Katz, E.; Willner, I. *J. Chem. Soc., Chem. Comm.* **1994**, 2741.

(10) Willner, I.; Doron, A.; Katz, E.; Levi, S.; Frank, A. J. *Langmuir* **1996**, *12*, 946.

(11) Willner, I.; Blonder, R.; Dagan, A. *J. Am. Chem. Soc.* **1994**, *116*, 9365.

(12) Blonder, R.; Levi, S.; Tao, G.; Ben-Dov, I.; Willner, I. *J. Am. Chem. Soc.* **1997**, *119*, 10467.

(13) Gabrielli, C. *Use and Application of Electrochemical Impedance Techniques*; Farnborough, 1990.

(14) (a) Bard, A. J.; Faulkner, L. R. *Electrochemical Methods: Fundamentals and Applications*; Wiley: New York, 1980. (b) Stoynov, Z. B.; Grafov, B. M.; Savova-Stoynov, B. S.; Elkin, V. V. *Electrochemical Impedance*; Nauka: Moscow, 1991.

(15) (a) Ren, X.; Pickup, P. G. *J. Electroanal. Chem.* **1997**, *420*, 251. (b) Hall, E. A. H.; Skinner, N. G.; Jung, C.; Szunerits, S. *Electroanalysis* **1995**, *7*, 830. (c) Skinner, N. G.; Hall, E. A. H. *Synthetic Metals* **1994**, *63*, 133. (d) Brillas, E.; Cabot, P. L.; Garrido, A.; Montilla, M.; Rodriguez, R. M.; Carrasco, J. *J. Electroanal. Chem.* **1997**, *430*, 133. (e) Ehret, R.; Baumann, W.; Brischwein, M.; Schwinde, A.; Stegbauer, K.; Wolf, B. *Biosens. Bioelectron.* **1997**, *12*, 29. (f) Janek, R. P.; Fawcett, W. R.; Ulman, A. *J. Phys. Chem.* **1997**, *101*, 8550.

(16) (a) Knichel, M.; Heiduschka, P.; Beck, W.; Jung, G.; Göpel, W. *Sens. Actuators B* **1995**, *28*, 85. (b) Rickert, J.; Göpel, W.; Beck, W.; Jung, G.; Heiduschka, P. *Biosens. Bioelectron.* **1996,** *11*, 757.

(17) Athey, D.; Ball, M.; McNeil, C. J.; Armstromg, R. D. *Electroanalysis* **1995**, *7*, 270.

(18) Doron, A.; Katz, E.; Tao, G.; Willner, I. *Langmuir* **1997**, *13*, 1783.

(19) Willner, I.; Doron, A.; Katz, E.; Levi, S.; Frank, A. J. *Langmuir* **1996**, *12*, 946.

(20) Woods, R.; Rand, D. A. *J. Electroanal. Chem.* **1971**, *31*, 29.

(21) (a) Randles, J. *Discuss. Faraday Soc.* **1947**, *1*, 11. (b) Ershler, B. V. *Discuss. Faraday Soc.* **1947**, *1*, 269.

(22) Champagne, G. Y.; Belanger, D.; Fortier, G. *Bioelectrochem. Bioenerg.* **1989**, *22*, 159.

(23) (a) Finklea, H. O.; Avery, S.; Lynch, M.; Furtsch, T. *Langmuir* **1987**, *3*, 409. (b) Sondag-Huethorst, J. A. M.; Fokkink, L. G. J. *Langmuir* **1992**, *8*, 2560.

(24) Delahay, P. In *Double Layer and Electrode Kinetics: Advances in Electrochemistry and Engineering;* Delahay, P., Tobias, C.W., Eds.; Wiley Interscience: New York, 1965; Chapter 3.

(25) (a) Lane, R. F., Hubbard, A. T. *J. Phys. Chem.* **1973**, *77*, 1401. (b) Lane, R. F.; Hubbard, A. T. *J. Phys. Chem.* **1973**, *77*, 1411. (c) Malem, F., Mandler, D. *Anal. Chem.* **1993**, *65*, 37. (d) Takehara, K.; Ide, Y. *Bioelectrochem. Bioenerg.* **1992**, *27*, 207. (e) Takehara, K.; Takemura, H.; Aihara, M.; Yoshimura, M. *J. Electroanal. Chem.* **1996**, *404*, 179. (f) Katz, E.; Schlereth, D. D.; Schmidt, H.-L. *J. Electroanal. Chem.* **1994**, *367*, 59.

(26) Katz, E.; Willner, I. *J. Electroanal. Chem.* **1996**, *418*, 67.

(27) Blonder, R.; Katz, E.; Cohen, Y.; Itzhak, N.; Riklin, A.; Willner, I. *Anal. Chem.* **1996**, *68*, 3151.

(28) (a) Degani, Y.; Heller, A. *J. Phys. Chem.* **1987**, *91*, 1285. (b) Schuhmann, W.; Ohara, T. J.; Schmidt, H.-L.; Heller, A. *J. Am. Chem. Soc.* **1991**, *113*, 1394. (c) Badia, A.; Carlini, R.; Fernandez, A.; Battaglini, F.; Mikkelsen, S. R.; English, A. M. *J. Am. Chem. Soc.* **1993**, *115*, 7053.

(29) Wilson, R.; Turner, A. P. F. *Biosens. Bioelectron.* **1992**, *7*, 165.

(30) Kato, S.; Aizawa, M.; Suzuki, S. *J. Membr. Sci.* **1976**, *1*, 289.

(31) Calvo, E. J.; Etchenique, R.; Danilowicz, C.; Diaz, L. *Anal. Chem.* **1996**, *68*, 4186.